Chinese Journal of Natural Medicines

**Pinoresinol diglucoside from *Eucommia ulmoides* attenuates diabetic cardiomyopathy through suppressing the store-operated calcium entry and downregulating the STIM1/Orai1/NFAT3 signaling pathway**

Yujie Feng, Yanan Mao, Junshuai Li, Zhipeng Sun, Yingchao Wang, Xinru Wang, Feng Wang, Tiantian Liu, Lane Zhang

**Citation:** Yujie Feng, Yanan Mao, Junshuai Li, Zhipeng Sun, Yingchao Wang, Xinru Wang, Feng Wang, Tiantian Liu, Lane Zhang, Pinoresinol diglucoside from *Eucommia ulmoides* attenuates diabetic cardiomyopathy through suppressing the store-operated calcium entry and downregulating the STIM1/Orai1/NFAT3 signaling pathway, Chinese Journal of Natural Medicines, 2026, 24(7), 849-858. doi: 10.1016/S1875-5364(26)61114-4.

View online: https://doi.org/10.1016/S1875-5364(26)61114-4

## Related articles that may interest you

*Eucommia* lignans alleviate the progression of diabetic nephropathy through mediating the AR/Nrf2/HO-1/AMPK axis *in vivo* and *in vitro*

Chinese Journal of Natural Medicines. 2023, 21(7), 516-526 https://doi.org/10.1016/S1875-5364(23)60427-3

Icariin attenuates vascular endothelial dysfunction by inhibiting inflammation through GPER/Sirt1/HMGB1 signaling pathway in type 1 diabetic rats

Chinese Journal of Natural Medicines. 2024, 22(4), 293-306 https://doi.org/10.1016/S1875-5364(24)60618-7

Jujuboside A ameliorates tubulointerstitial fibrosis in diabetic mice through down-regulating the YY1/TGF-$\beta$1 signaling pathway

Chinese Journal of Natural Medicines. 2022, 20(9), 656-668 https://doi.org/10.1016/S1875-5364(22)60200-0

Bavachin induces apoptosis in colorectal cancer cells through Gadd45a *via* the MAPK signaling pathway

Chinese Journal of Natural Medicines. 2023, 21(1), 36-46 https://doi.org/10.1016/S1875-5364(23)60383-8

Qi-Tai-Suan, an oleanolic acid derivative, ameliorates ischemic heart failure *via* suppression of cardiac apoptosis, inflammation and fibrosis

Chinese Journal of Natural Medicines. 2022, 20(6), 432-442 https://doi.org/10.1016/S1875-5364(22)60156-0

Cyasterone inhibits IL-1$\beta$-mediated apoptosis and inflammation *via* the NF-$\kappa$B and MAPK signaling pathways in rat chondrocytes and ameliorates osteoarthritis *in vivo*

Chinese Journal of Natural Medicines. 2023, 21(2), 99-112 https://doi.org/10.1016/S1875-5364(23)60388-7

Wechat

Chinese Journal of Natural Medicines 24 (2026) 849-858

Contents lists available at ScienceDirect

Chinese Journal of Natural Medicines

journal homepage: www.cjnmcpu.com/



Original article

# Pinoresinol diglucoside from *Eucommia ulmoides* attenuates diabetic cardiomyopathy through suppressing the store-operated calcium entry and downregulating the STIM1/Orai1/NFAT3 signaling pathway

Yujie Feng[a,Δ], Yanan Mao[a,Δ], Junshuai Li[a,Δ], Zhipeng Sun[b,Δ], Yingchao Wang[a], Xinru Wang[a], Feng Wang[b], Tiantian Liu[c], Lane Zhang[a,*]

[a] *School of Nursing, Shandong Second Medical University, Weifang 261053, China*
[b] *School of Pharmacy, Shandong Second Medical University, Weifang 261053, China*
[c] *Dongfang Hospital, Beijing University of Chinese Medicine, Beijing 100078, China*

ARTICLE INFO

*Article history:*
Received 5 May 2025
Revised 19 August 2025
Accepted 6 January 2026
Available online 20 July 2026

*Keywords:*
Pinoresinol diglucoside (PDG)
Diabetic cardiomyopathy (DCM)
Store-operated calcium entry (SOCE)
STIM1/Orai1/NFAT3 signaling pathway
Cardiac hypertrophy
Inflammation and apoptosis

ABSTRACT

Pinoresinol diglucoside (PDG), an active component derived from *Eucommia ulmoides*, exhibits therapeutic effects against apoptosis, inflammation, and hypertrophy, etc. However, whether PDG plays a protective role in diabetic cardiomyopathy (DCM) is not fully elucidated. This study aimed to investigate the role and potential mechanism of PDG in DCM. The possible mechanism of PDG targeting DCM was identified by network pharmacology, bioinformatics, machine learning and molecular docking methods. The heart function of mice was evaluated using echocardiography. The pathological changes in the heart of mice were detected using H&E staining. Changes of $Ca^{2+}$ fluorescence intensity values in H9c2 cells were assessed by confocal microscopy. Apoptosis was evaluated by TUNEL staining and flow cytometry. The expression of DCM-related genes and proteins, both *in vivo* and *in vitro*, was examined by qRT-PCR and Western blot. The results showed that PDG effectively improved the cardiac function and suppressed cardiac hypertrophy, inflammation, and cardiomyocyte apoptosis caused by DCM. Intriguingly, molecular docking results revealed that the therapeutic effect of PDG on DCM was associated with stromal interaction molecule 1 (STIM1), calcium release-activated calcium channel protein 1 (Orai1), and nuclear factor of activated T-cells 3 (NFAT3) signaling. Consistently, animal experiments results indicated that PDG significantly downregulated the expression of STIM1, Orai1, NFAT3 at the protein level, as well as the associated store-operated calcium entry (SOCE). Therefore, our findings revealed that PDG can alleviate cardiac hypertrophy, inflammation and apoptosis in DCM by downregulating the STIM1, Orai1, and NFAT3 signaling molecules. Thus, PDG may be a promising therapeutic candidate for treating DCM.

## 1. Introduction

Diabetic cardiomyopathy (DCM) is a common myocardial complication accompanied by ventricular dysfunction and structural abnormalities in patients with diabetes mellitus (DM) without coronary artery disease, valve diseases, and hypertension [1]. It is characterized by cardiac hypertrophy, fibrosis, inflammation, oxidative stress, apoptosis, and dysregulation of calcium homeostasis in cardiomyocytes [2]. Specific therapeutic strategies or drugs are not available for treating DCM to date. Notably, Li et al. have recently reported the use of traditional Chinese medicine (TCM) for the treatment of DCM. TCM modulates multiple pathways and targets, with fewer side effects [3].

The mechanisms of diabetes-related cardiovascular complications are complex. Notably, altered endoplasmic reticulum (ER) $Ca^{2+}$ signaling plays a key role in the pathogenesis of diabetes [4]. Store-operated calcium entry (SOCE), an important $Ca^{2+}$ flux pathway in cardiomyocytes, is mainly composed of stromal interaction molecule 1 (STIM1) and calcium release-activated calcium channel modulator 1 (Orai1) [5]. STIM1 is an ER $Ca^{2+}$ sensor, which functions to monitor and replenish ER-luminal $Ca^{2+}$ level through SOCE, and Orai1 is mainly involved in the formation of $Ca^{2+}$ pathways in the cell membrane [6]. STIM1 and its isoform (STIM1L) enhance SOCE and participate in the pathogenesis of pathological cardiac hypertrophy [7]. In neonatal rat ventricular myocytes, short-term hyperglycemia suppressed SOCE induced by angiotensin II (Ang II) or thapsigargin (TG) [8]. Previous study demonstrated that platelets from type 2 DM (T2DM) patients with peripheral artery disease (PAD) exhibited a significant increase in SOCE and the up-regulation of STIM1 and SERCA3 [9]. Moreover, the deficiency of *Orai1* can block hypertrophic signaling in pathologically hypertrophic cardiomyocyte [10]. Furthermore, the increase of SOCE can activate a number of $Ca^{2+}$-dependent enzymes and transcription factors including nuclear factor of activated T cells (NFAT) [11], leading to myocardial hypertrophy, apoptosis, fibrosis, etc [12]. Additionally, the activation of NFAT3 plays an important role in the

* Corresponding author.
*E-mail address:* nzh149@126.com (L. Zhang)
Δ These authors contributed equally to this work.

https://doi.org/10.1016/S1875-5364(26)61114-4
Copyright © 2026, China Pharmaceutical University. Published by Elsevier B.V. All rights are reserved.

development of diabetes-related cardiovascular complications [13]. Therefore, it was speculated that the STIM1/Orai1/NFAT3 signaling may be a therapeutic target in inhibiting the progression of DCM.

*Eucommia ulmoides* (http://www.theplantlist.org), a TCM being tonifying the liver and kidneys and strengthening the sinews and bones has the multiple therapeutic effects, such as antihypertension, anti-oxidation, anti-inflammatory, and the ability of reducing blood glucose and lipids [14]. Additionally, chlorogenic acid extracted from *Eucommia ulmoides* has the cardioprotective role in cardiovascular diseases [15]. Therefore, these evidences indicate that *Eucommia ulmoides* with dual pharmacological properties of regulating metabolism and protecting the heart, is associated with the core pathological mechanism of DCM. Pinoresinol diglucoside (PDG), a lignan from *Eucommia ulmoides*, has many pharmacologic properties, such as anti-hypertensive, anti-endothelial dysfunction, anti-inflammation, and anti-oxidant properties [16, 17]. In addition, it can ameliorate cardiomyocyte injury related to myocardial ischemia/reperfusion [18]. In a rat model, PDG exerts a cardioprotective role in attenuating cardiac hypertrophy by downregulating the Akt/mTOR/NF-κB pathway induced by pressure overload [19]. However, whether PDG has a protective role in DCM is not fully elucidated. Rosiglitazone (Rosi), a peroxisome proliferator-activated receptor agonist, can improve lipid metabolism disorders in diabetic organisms, and alleviate myocardial damage caused by T2DM [20]. Moreover, it is reported that Rosi is a positive drug to validate the effect of Chinese medicine such as Zhilong Huoxue Tongyu Capsule on DCM [21]. Herein, Rosi was regarded as a positive drug to identify the therapeutic effect of PDG in treating DCM.

Recently, network pharmacology, bioinformatics analysis, machine learning and molecular docking methods have played key roles in exploring the therapeutic targets of TCM for diseases [22]. In this study, we used network pharmacology, bioinformatics, machine learning and molecular docking methods to identify the potential mechanism by which PDG targets DCM. Furthermore, we used an *in vivo* mouse model (db/db mice) and an *in vitro* cell model (high glucose-stimulated H9c2 cells) of DCM to determine the effect of PDG on DCM induced by T2DM. Interestingly, we investigated whether the action of PDG on DCM was mediated by the STIM1/Orai1/NFAT3 pathway and its associated SOCE.

## 2. Materials and methods

### 2.1. Preparation of PDG and rosiglitazone (Rosi)

PDG (#63902-38-5; MW 682.67) with a purity of > 99% was purchased from Chengdu Manster Biotechnology Co. Ltd. (Chengdu, China). PDG (2 mg·mL$^{-1}$) and Rosi (20 μmol·L$^{-1}$, #HY-17386, MedChemExpress, NJ, USA) solutions were prepared for the subsequent experiments.

### 2.2. Chemicals and antibodies

Dulbecco's modified eagle's medium (DMEM, #6124116) was obtained from GIBCO Laboratories (Grand Island, NY, USA). Fetal bovine serum (FBS) was acquired from BOVOGEN Laboratories (#2211C, Melbourne, Australia). BCA protein assay reagent was obtained from Thermo (#23227, MA, USA). Cocktail was procured from Sigma Chemical Co. (#G2006, St. Louis, MO). Lipo8000™ Transfection Reagent was obtained from Beyotime Biotech Co., Ltd. (#C0533, Shanghai, China). The primary antibodies were as follows: STIM1 (#5668, 1∶1000), caspase 8 (#4790, 1∶1000), caspase 3 (#14220, 1∶1000) and NFAT3 (#2183, 1∶1000) were purchased from CST (MA, USA); Orai1 (sc-377281, 1∶500) was obtained from Santa Cruz Biotechnology (CA, USA); GAPDH (#60004-1, 1∶2000) was purchased from Proteintech (Chicago, USA). The rabbit secondary antibody (SA00001-2, 1∶8000) and mouse secondary antibody (SA00001-1, 1∶8000) were purchased from Proteintech (Chicago, USA). TUNEL BrightGreen Apoptosis Detection Kit (A112-01, Vazyme Biotech Co., Ltd., Nanjing, China), BD Pharmingen™ FITC Annexin V Apoptosis Detection Kit I (#556547, BD Biosciences, San Jose, CA) and Fluo-4, AM (F14201, Invitrogen, USA) were obtained commercially. The synthesis of primers *Anp*, *Bnp*, *β-Mhc*, *Il-1β*, *Il-6*, *Tnf-α*, and *Gapdh* was performed by Sangon Bio (Shanghai, China) from ZSGB-BIO. The small interfering RNA (siRNA) targeting *Stim1* or *Orai1* was synthesized by Gene Pharma Co. Ltd. (Shanghai, China).

### 2.3. Animals

Male db/db (C57BLKS/J) mice, aged 8 weeks and weighing 35–40 g, were purchased from Cytogen Bio (Hebei, China). The control mice were db/m mice of the same strain. Mice were kept in the animal center of Shandong Second Medical University at 22 ± 1 °C and 60% ± 10% relative humidity in a 12h/12h light/dark cycle. The animals were allowed unrestricted access to water and food. The experiments were carried out according to the requirements set forth in the "Care and Use of Laboratory Animals" by the People's Government of Shandong Province, as well as the guidelines of the National Institutes of Health. The experimental protocol was approved by the Laboratory Animal Ethics Committee of Shandong Second Medical University (No. 2021SDL400).

### 2.4. Animal grouping and drug administration

Fifty db/db mice were randomly divided into five groups ($n$ = 10/each group): (1) model group: treated with the vehicle (saline); (2) PDG-L group: treated with the low dose of PDG (1 mg·kg$^{-1}$·d$^{-1}$); (3) PDG-M group: treated with the medium dose of PDG (2.5 mg·kg$^{-1}$·d$^{-1}$); (4) PDG-H group: treated with the high dose of PDG (5 mg·kg$^{-1}$·d$^{-1}$); (5) Rosi-treated group: treated with Rosi (2 mg·kg$^{-1}$·d$^{-1}$). The control group was male db/m mice of the same strain as db/db mice, treated with the vehicle (saline). All drugs of PDG or Rosi were intraperitoneally administered to all animals once daily for 8 weeks.

### 2.5. Echocardiography

Using a VEVO 2100 imaging system (Visual Sonics Inc., Toronto, Canada), mice heart function was evaluated after anesthetized with isoflurane. The left ventricular ejection fraction (LVEF), left ventricular fraction shortening (LVFS), thickness of the left ventricle posterior wall in diastole (LVPWd) and systolic (LVPWs), and thickness of the left ventricle internal diastolic in diameter (LVIDd) were used to determine whether mice appeared cardiac dysfunction. At least three consecutive measurements were recorded for all echocardiographic parameters.

### 2.6. Histological analysis

The ventricular tissues of heart in mice were harvested, further fixed overnight in 4% paraformaldehyde, dehydrated, and finally embedded. Sections (5-μm thickness) were used to perform the experiments for H&E staining and TUNEL assay. Images were captured under a light microscope (DM48, Leica, Germany) and analyzed using the Image J software (v1.53t, NIH, USA).

### 2.7. Cell culture and drug administration

H9c2 cells were provided by the laboratory of Dr. Luo, Capit-

al Medical University, China. The cells were cultured in low-sugar DMEM supplemented with 10% FBS and 1% penicillin-streptomycin (#G4003, Solarbio, Wuhan, China) at 37 °C and 5% carbon dioxide. The cells were exposed to 33.3 mmol·L$^{-1}$ glucose to mimic the condition of DCM, whereas control cells were exposed to 5.5 mmol·L$^{-1}$ glucose. Subsequently, glucose-exposed cells were treated with PDG (2.5, 5, and 7.5 μg·mL$^{-1}$) or Rosi (20 μmol·L$^{-1}$).

### 2.8. Screening of PDG and DCM targets

The chemical structure of PDG was obtained from the PubChem database (https://pubchem.ncbi.nlm.nih.gov/). Potential target genes for PDG were identified using the PharmMapper and Swiss Target Prediction databases (http://swisstargetprediction.ch/). After merging the genes and removing duplicates, the final drug target genes were determined. The DCM-related targets were retrieved from the GeneCards (https://www.genecards.org/) and Online Mendelian Inheritance in Man (OMIM) (https://omim.org/) databases. These targets were merged, while the duplicates were removed in order to obtain the final set of DCM-related targets. The intersection of PDG-related genes and DCM-related genes was extracted. The Venn diagram was obtained using the R package "ggvenn".

### 2.9. Acquisition of differential expressed genes (DEGs)

After downloading the DCM-related datasets from the Gene Expression Omnibus (GEO) database (https://www.ncbi.nlm.nih.gov/geo), we merged them using *R* software (Version 4.5.1) and obtained principal component analysis (PCA) plots. Using the *R* package "limma", we achieved DEGs with the screening criteria of $P < 0.05$ and $|\log_2 (FC)| > 0.262$. Furthermore, a volcano plot of DEGs using the *R* package "ggplot2" was obtained.

### 2.10. GO and KEGG enrichment analysis

Herein, the enrichment analysis of GO and KEGG pathway on the targets of PDG on DCM was conducted using the *R* package "cluster profiler package and org.Hs.eg.db". The significance was regarded as $P < 0.05$. The bar charts and bubble charts were obtained using the *R* package "ggplot2".

### 2.11. Screen core genes using machine learning algorithms

Using two machine learning algorithms, least absolute shrinkage and selection operator (LASSO) regression and support vector machine-recursive feature elimination (SVM-RFE), the core targets of PDG on DCM were identified. The LASSO regression model was constructed using the *R* package "glmnet", and the SVM-RFE adopted the *R* package "e1071" to analyze the minimum point after cross-validation and output the corresponding genes. The final feature genes were obtained by taking the intersection of the feature genes selected by LASSO regression and SVM-RFE methods.

### 2.12. Molecular docking

The molecular structure of PDG was obtained from the PubChem database, while the protein structures of the core targets were retrieved from the Protein Data Bank (PDB; http://www.rcsb.org/). Molecular docking simulation calculations were performed through the AutoDock tool, and the final visual analysis was conducted using PyMol 3.1 software. The predicted binding constant was calculated to evaluate the binding energy. When the binding energy between two molecules is ≤ −5 kcal·mol$^{-1}$, it indicates that there is a strong binding affinity between them [23].

### 2.13. Cytosolic $Ca^{2+}$ measurement

Fluo4-AM powder (50 μg) was dissolved in DMSO (11.395 μL) to prepare the Fluo4-AM masterbatch (4 mmol·L$^{-1}$). Fluo4-AM master mix was diluted with serum-free DMEM to make a 4 μmol·L$^{-1}$ working solution. The cells were treated with Fluo 4-AM and incubated at 37 °C for 40 min. Finally, the cells were gently washed with calcium-free HEPES solution (NaCl: 0.788 g, KCl: 0.038 g, $MgCl_2$: 0.02 g, HEPES: 0.238 g, Glucose: 0.218 g; pH 7.2).

A laser confocal microscope (TCS SP8, Leica, Germany) was used to analyze relevant parameters. The initial fluorescence intensity of intracellular $Ca^{2+}$ ions (F0) was recorded by selecting the appropriate cell level. After the cells were stabilized, 2 μmol·L$^{-1}$ of TG was added, and the resulting change in the fluorescence intensity of the $Ca^{2+}$ release (F) was continuously recorded. When the calcium signal of the cells returned to the resting state, a 1.8 mmol·L$^{-1}$ $CaCl_2$ solution was added, and the change in fluorescence intensity of the transient $Ca^{2+}$ inflow was recorded (F) until the cells returned to the resting state. The ratio of the change in fluorescence intensity of $Ca^{2+}$ ions to the initial fluorescence intensity of $Ca^{2+}$ ions in each cell (F/F0) was determined.

### 2.14. Quantitative real-time PCR (qRT-PCR)

Total RNA was isolated from mouse heart tissues or H9c2 cells and reverse transcribed using a reverse transcription kit (FSQ-101, TOYOBO, Japan). qRT-PCR was performed using SYBR Green Realtime PCR Master Mix (QPK-201, TOYOBO, Japan) and Light Cycler® 480 (Roche, Germany). Supplemental Table S1 showed the primers of target genes. The gene expression was detected by the $2^{-\Delta\Delta Ct}$ method.

### 2.15. Western blot

The BCA protein assay kit was used to determine the protein content in mouse heart tissues and H9c2 cells. The electrophoresed proteins were transferred onto a PVDF membrane. The membranes were blocked with milk (5%) and then incubated with different primary antibodies at 4 °C for more than 12 h. Finally, the membranes were incubated with the secondary antibody at room temperature for 1 h. The protein bands were analyzed and quantified using an e-BLOT Touch Imager (e-BLOT, China).

### 2.16. siRNA transfection

H9c2 cells were cultured at a density of 1.2 × 10$^5$/well in a 6-well plate (cell confluence: 60%–70%) and further transfected with si*Stim1* or si*Orai1* (50 nmol·L$^{-1}$). The transfection mix was composed of 125 μL serum-free low-glycemic DMEM, 5 μL small interference stock solution, and 4 μL Lipo8000™ Transfection reagent. After transfection for 24 h, the cells were exposed to HG with the simultaneous addition of three different PDG doses (2.5, 5, and 7.5 μg·mL$^{-1}$) for 24 h. Finally, the cells were harvested for subsequent experiments. The sequences of si*Stim1* and si*Orai1* are listed in Supplemental Table S2.

### 2.17. Flow cytometry

The rates of cell apoptosis were determined using BD Pharmingen™ FITC Annexin V Apoptosis Detection Reagent. H9c2 cells were digested with 0.25% trypsin, collected, and rinsed twice with PBS. Subsequently, cells were mixed with 1 × binding buffer suspension, FITC Annexin V, and PI and incubated at 25 °C for 15 min away from light. Analysis was conducted within 1 h using a flow cytometer-C6 plus (BD Biosciences,

USA).

### 2.18. Statistical analysis

Statistical analysis and graphing were conducted using GraphPad Prism 9.5.1 software (San Diego, USA). All data were indicated as mean ± standard deviation (SD). Comparisons among multiple groups were analyzed using one-way ANOVA, followed by Tukey's test. $P < 0.05$ was considered statistically significant.

## 3. Results

### 3.1. PDG alleviated cardiac dysfunction caused by T2DM

According to the previous study [24], we used leptin receptor-deficient db/db mice as the mouse model of DCM in order to mimic the development of T2DM-related cardiac complications. Mouse heart tissues were harvested for further analysis after PDG or Rosi treatment for 8 weeks (Fig. 1A). Echocardiographic data revealed that db/db mice had a lower level of the LVEF and LVFS than db/m mice. However, PDG or Rosi treatment reversed these changes (Figs. 1B–1D). Meanwhile, LVPWd and LVPWs were significantly increased in db/db mice rather than db/m mice, while PDG treatment inhibited this kind of change in the corresponding groups (Figs. 1E and 1F). A similar trend was observed in LVIDs value (Fig. 1G). However, there was no significant difference between PDG and Rosi treatment. These findings indicated that PDG was effective in attenuating cardiac dysfunction in db/db mice.

### 3.2. PDG ameliorated cardiac hypertrophy, inflammation and apoptosis in db/db mice

In this study, the heart size was much larger in db/db mice relative to db/m mice, and this alteration was markedly mitigated by PDG or Rosi treatment (Fig. 1H). Furthermore, the ratio of HW/TL was as well as higher in db/db mice compared with the control mice, and PDG or Rosi treatment reversed this kind of change (Fig. 1I). db/db mice exhibited a much larger cross-sectional area than db/m mice, PDG or Rosi decreased this increase in area (Figs. 1H, and 1J). The expression of hypertrophic markers (*Anp*, *Bnp*, and *β-Mhc*) at the mRNA level was significantly increased in db/db mice relative to db/m mice, and PDG administration obviously reversed these above changes, especially the PDG-H treatment showed the most pronounced reduction (Figs. 1K–1M). Moreover, PDG effectively suppressed the inflammatory response (*Il-6*, *Tnf-α*, and *Il-1β*) at the mRNA level, and the PDG-H-treatment exhibited the most optimal efficiency (Figs. 2A–2C). Herein, db/db mice had more apoptotic cells than db/m mice. PDG effectively reversed these changes, and the PDG-H-treated group exhibited the optimum effect (Figs. 2D and 2E). PDG down-regulated the expression of the related apoptotic proteins (cleaved caspase-8/caspase-8 and cleaved caspase-3/caspase-3), and PDG-H treatment exhibited the strongest inhibitory effect (Figs. 2F–2I). To sum up, these data suggested that PDG was effective in suppressing T2DM-related cardiac hypertrophy, inflammation and apoptosis.

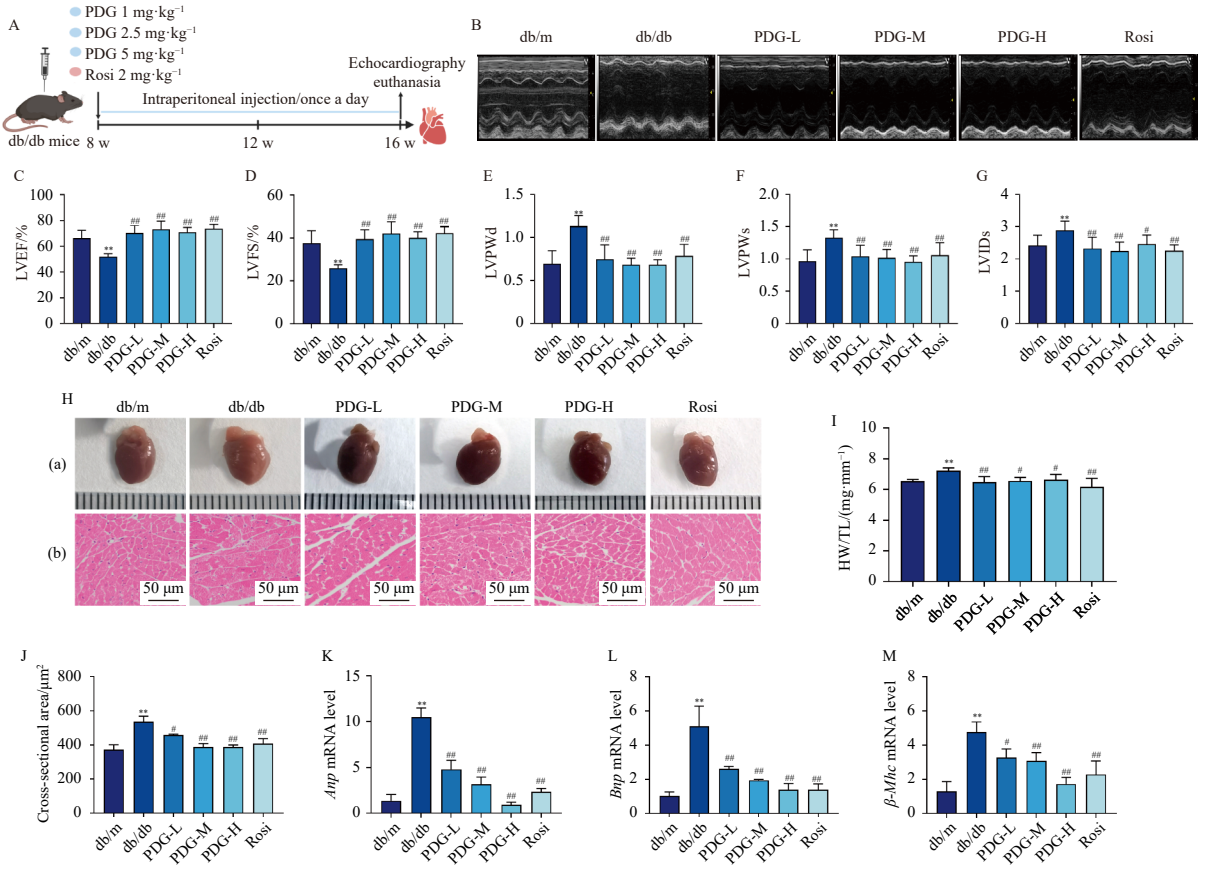



**Fig. 1** PDG alleviated cardiac dysfunction and cardiac hypertrophy in db/db mice. (A) Experimental protocol of PDG on the *in vivo* mouse model of DCM ($n = 10$). (B) Representative echocardiographic images of mice. (C–G) Quantification of echocardiogram parameters ($n = 9–10$). LVEF, left ventricular ejection fraction; LVFS, left ventricular fractional shortening; LVPWd, left ventricular posterior wall diastole; LVPWs, left ventricular posterior wall systole; LVIDs, left ventricle internal diastolic systole. (H) Typical heart images: (a) Representative images of heart sizes. (b) HE staining typical images (scale bar = 50 μm). (I) The ratio of heart weight to tibia length (HW/TL) ($n = 6$). (J) Left ventricular cardiomyocyte area ($n = 3$). (K–M) Relative mRNA expression levels of *Anp*, *Bnp*, *β-Mhc* in heart tissues of mice, determined by qRT-PCR ($n = 4$). Data are shown as mean ± SD. One-way ANOVA, $^{*}P < 0.05$, $^{**}P < 0.01$ *vs* db/m group; $^{\#}P < 0.05$, $^{\#\#}P < 0.01$ *vs* db/db group. All experiments were repeated at least three times.

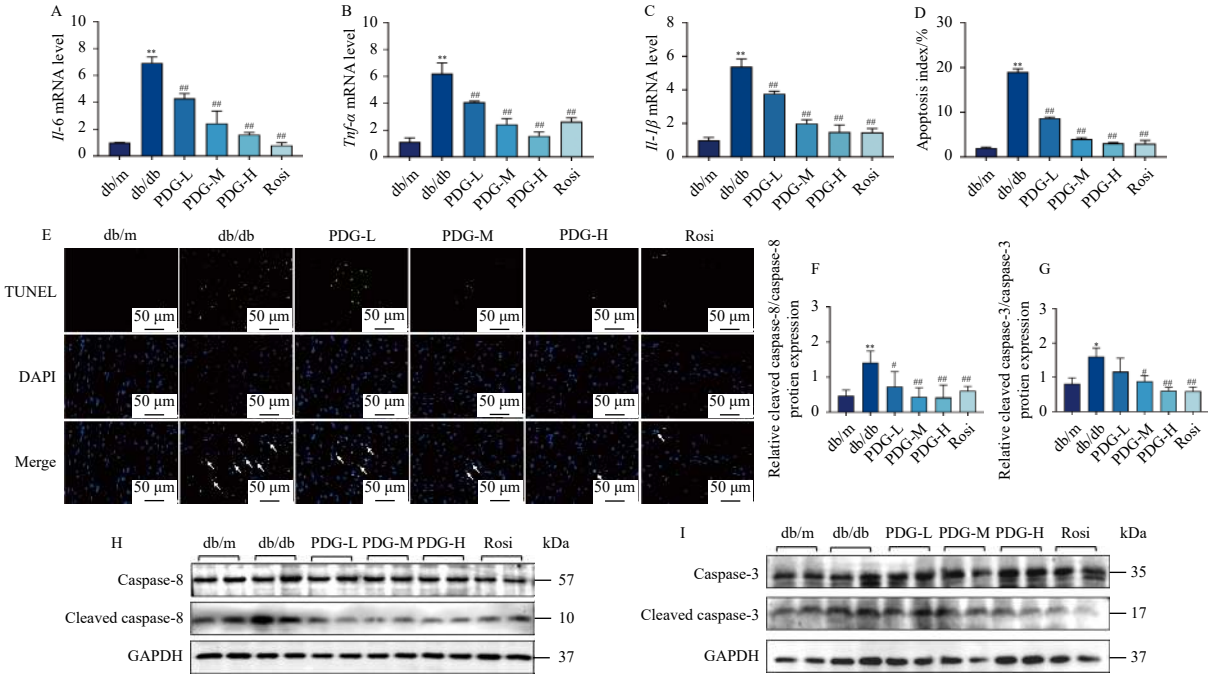



**Fig. 2** PDG ameliorated inflammation and apoptosis in db/db mice. (A–C) Relative mRNA levels of *Il-6*, *Tnf-α*, and *Il-1β* in heart tissues of mice ($n$ = 4). (D) Quantification of TUNEL-stained positive cells ($n$ = 3). (E) The representative images of mouse heart tissues with TUNEL (green) staining and DAPI (blue) nuclear staining. White arrows indicate apoptotic-positive cells (scale bar = 50 μm). (F–I) Quantification and Western blotting of caspase-8, cleaved caspase-8, caspase-3, cleaved caspase-3 protein expressions in mouse hearts ($n$ = 4). Data are shown as mean ± SD. One-way ANOVA, $^{*}P < 0.05$, $^{**}P < 0.01$ *vs* db/m group; $^{\#}P < 0.05$, $^{\#\#}P < 0.01$ *vs* db/db group. All experiments were repeated at least three times.

### *3.3. PDG suppressed cardiac hypertrophy, inflammation, and apoptosis in HG-induced H9c2 cells*

To further identify whether PDG had the inhibitory effect on DCM *in vitro*, we used HG-induction to establish the cellular DCM model (Fig. 3A). As shown in Figs. 3B–3D, PDG effectively suppressed cardiac hypertrophy in HG-induced H9c2 cells. Furthermore, PDG obviously inhibited the inflammatory response induced by HG (Figs. 3E–3G). Additionally, PDG also suppressed apoptosis induced by HG (Figs. 3H and 3I). Interestingly, the PDG-treated groups and Rosi-treated group exhibited a similar trend. Collectively, these data indicated that PDG had the similar inhibitory effect on DCM *in vitro*.

### *3.4. The results of network pharmacology and bioinformatics*

A total of 387 PDG-related targets were identified in the PharmMapper and Swiss Target Prediction databases. After re-

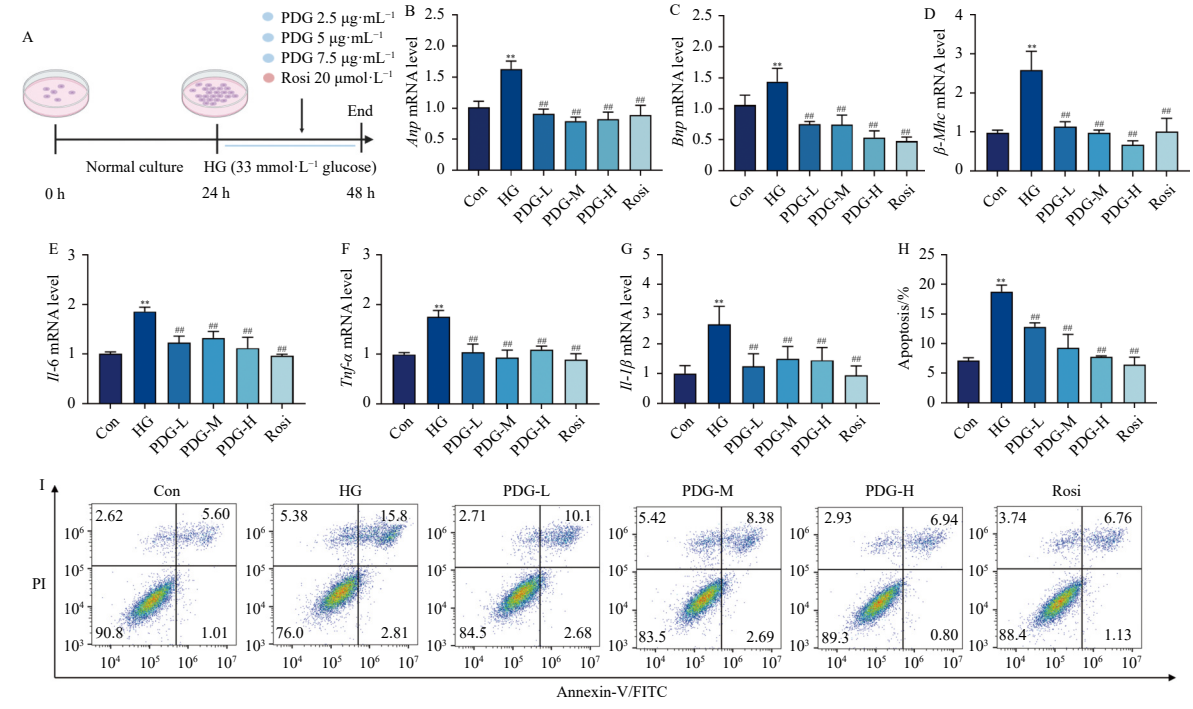



**Fig. 3** PDG suppressed cardiac hypertrophy, inflammation, and apoptosis induced by HG in H9c2 cells. (A) Experimental protocol of PDG on the *in vitro* cells model of DCM. H9c2 cells were exposed to HG (33.3 mmol·L$^{-1}$) for 24 h and treated with PDG (2.5, 5, and 7.5 μg·mL$^{-1}$) or Rosi (20 μmol·L$^{-1}$). (B–G) Relative mRNA expression levels of *Anp*, *Bnp*, *β-Mhc*, *Il-6*, *Tnf-α*, and *Il-1β* in H9c2 cells were measured by qRT-PCR ($n$ = 4). (H and I) Apoptosis was measured using flow cytometry in H9c2 cells ($n$ = 3). Data are shown as mean ± SD. One-way ANOVA, $^{*}P < 0.05$, $^{**}P < 0.01$ *vs* Con group; $^{\#}P < 0.05$, $^{\#\#}P < 0.01$ *vs* HG group. All experiments were repeated at least three times.

moving duplicates, 4052 DCM-related targets were obtained from the GeneCards and OMIM databases. As depicted in Fig. 4A, the intersection analysis of PDG on DCM was shown in the Venn diagram with 238 target genes. Furthermore, we downloaded the datasets of GSE26887 and GSE62203 from the GEO database, merged and normalized them, and removed the heterogeneity of the datasets before and after the batch effect (Figs. 4B and 4C). After analyzing the GSE26887 and GSE62203 datasets, 295 genes with significant differences were screened out. These genes were 170 up-regulated genes and 125 down-regulated genes. The top 50 genes with the greatest variations were shown in the volcano plot (Fig. 4D). The intersection of the DEGs and the PDG-DCM genes was extracted to obtain 11 genes, which were visualized using a Venn diagram (Fig. 4E). To explore the therapeutic effect of PDG on DCM, we further conducted the enrichment function analysis of GO and KEGG pathway on the 11 overlapping target genes. The top 10 GO terms in each category were selected for visualization. Biological process (BP) analysis revealed that the target genes were enriched in response to metal ion, purine ribonucleotide metabolic process, store-operated calcium entry, etc. The cellular components (CC) involved plasma membrane raft, ficolin-1-rich granule lumen, mitochondrial outer membrane, etc. In molecular functions (MF), genes were significantly enriched in monosaccharide binding, store-operated calcium channel activity, etc (Fig. 4F). KEGG enrichment analysis showed that glycolysis/gluconeogenesis, pentose phosphate pathway and calcium signaling pathway were the top three signaling pathways (Fig. 4G). These data indicated the action mechanism of PDG targeting DCM was possibly through the calcium signaling-related signaling pathway.

### 3.5. The results of machine learning screening

LASSO regression and triple cross-validation were conducted to screen out 8 potential key genes (Figs. 5A and 5B). SVM-RFE algorithm further identified 7 core genes (Figs. 5C and 5D). The Venn plot showed that the two algorithms identified a total of 6 overlapping genes related to PDG treating DCM, including glucose-6-phosphate isomerase (*Gpi*), receptor related orphan receptor alpha (*Rora*), heme oxygenase 1 (*Hmox1*), *Stim1*, *Nfat3*, and *Orai1* (Fig. 5E).

### 3.6. Molecular docking analysis of PDG and DCM targets

We further used molecular docking method to evaluate whether PDG had the interaction to STIM1/Orai1/NFAT3 signaling. The results showed that the binding energies of PDG with STIM1, Orai1, and NFAT3 were −7.6, −6.7, and −6.4 kcal·mol$^{-1}$, indicating that PDG had a strong binding affinity to STIM1, Orai1 and NFAT3 proteins (Figs. 5F–5H).

### 3.7. The inhibitory effect of PDG on DCM may be associated with the STIM1/Orai1/NFAT3 signaling and its associated SOCE

As shown in Figs. 6A and 6B, we identified the silencing effect of si*Stim1* and si*Orai1*. HG induced a significant increase of hypertrophic genes (*Anp*, *Bnp*, and *β-Mhc*) and inflammatory genes (*Il-6*, *Tnf-α*, and *Il-1β*) at mRNA level. In contrast, the deficiency of *Stim1* or *Orai1* reversed these changes, and no additive effect was observed after PDG treatment (Figs. 6C–6F). Additionally, the apoptosis rate increased in the HG-treated group. This rate decreased after silencing *Stim1* or *Orai1*. However, no additive effects were displayed in si*Stim1* or si*Orai1*-treated cells followed by HG-induction and PDG treatment (Figs. 6G–6I). Furthermore, we validated the action of PDG on SOCE caused by HG, followed by TG (2 μmol·L$^{-1}$) treatment to deplete the intracellular calcium ions and external calcium (1.8 mmol·L$^{-1}$) to induce an elevation of intracellular calcium in H9c2 cells. The amplitude of SOCE was significantly higher in the HG-induced cells than in the control cells, and PDG or Rosi treatment significantly reversed these changes (Figs. 7A and 7B). We noted a marked downregulation of STIM1 and Orai1 protein expression in db/db mice relative to the db/m mice after PDG or Rosi treatment (Figs. 7C, 7E and 7F). Furthermore, we validated the effect of PDG on

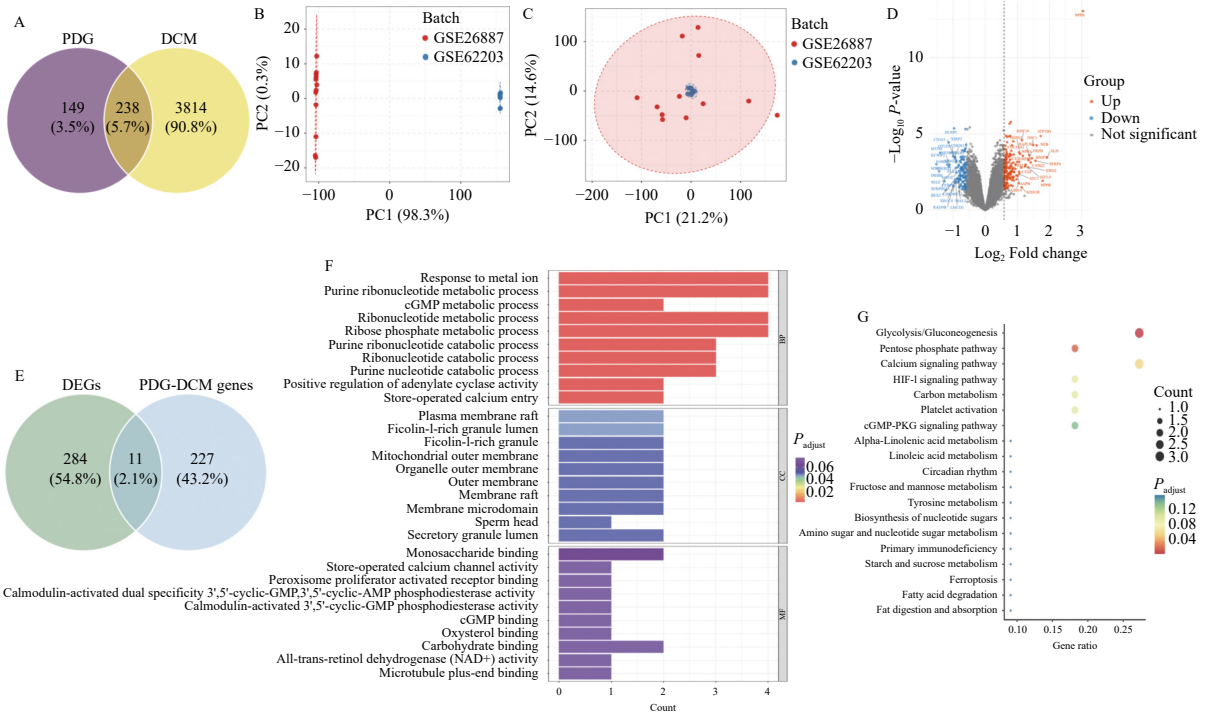



**Fig. 4** Analysis of potential target screening and pathway enrichment of PDG on DCM. (A) Venn diagram of PDG-related targets and DCM-related targets. (B) PCA before batch effects remove. (C) PCA after batch effects remove. (D) Volcano plot of DEGs. (E) Venn diagram of 295 DEGs and 238 PDG-DCM genes. (F) GO enrichment functional analysis. (G) KEGG enrichment functional analysis.

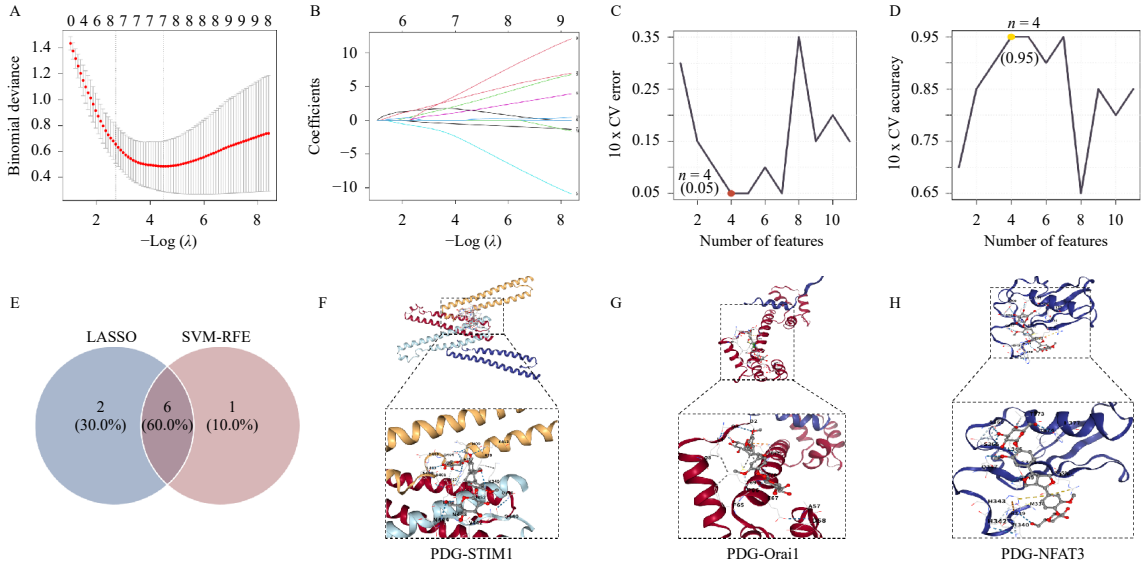



**Fig. 5** Analysis of core targets of PDG treating DCM using machine learning algorithms and molecular docking. (A) The cross-validation diagram of LASSO analysis. (B) The regression diagram of LASSO analysis. (C) Generalization error *vs* Number of features. (D) CV accuracy *vs* Number of features. (E) Venn diagram of the overlapping part between LASSO and SVM-RFE. (F) The molecular docking diagram of PDG and STIM1. (G) The molecular docking diagram of PDG and Orai1. (H) The molecular docking diagram of PDG and NFAT3.

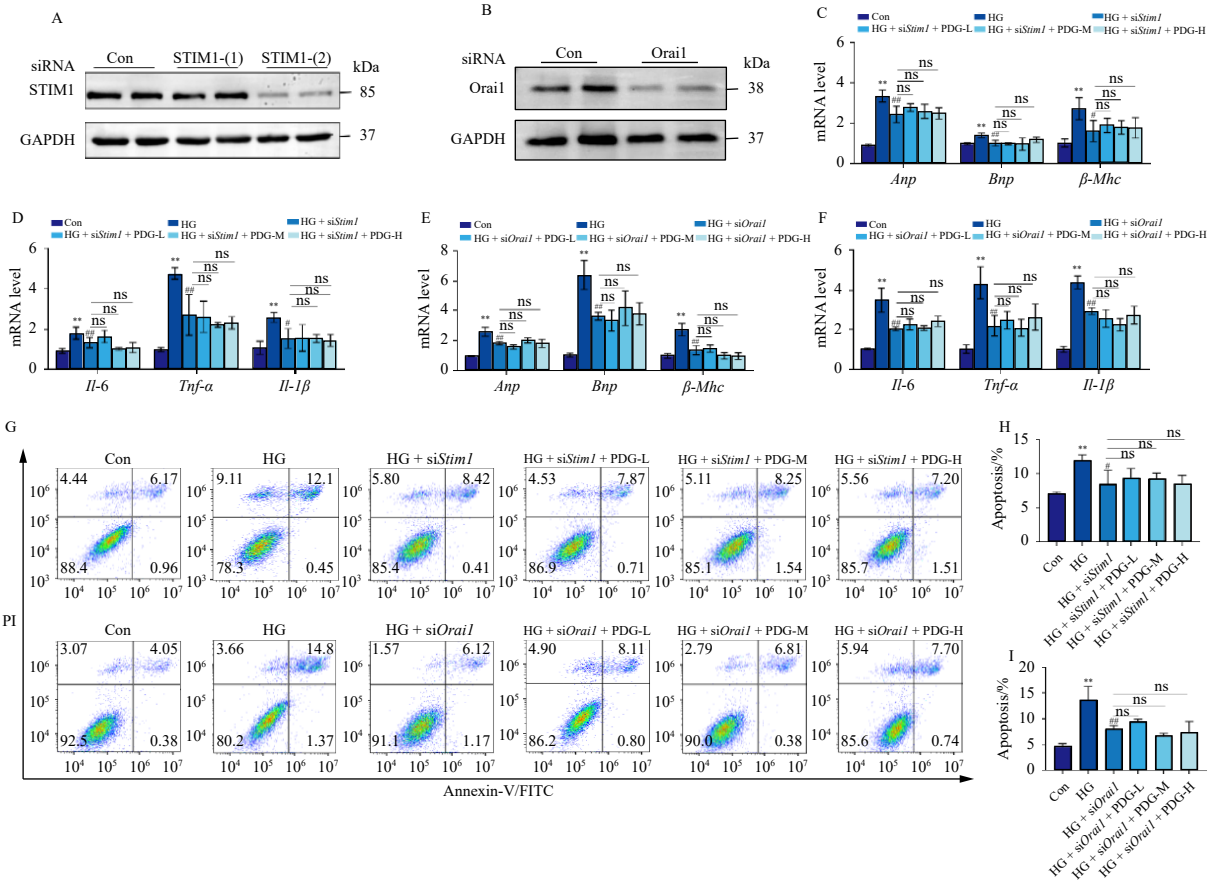



**Fig. 6** The inhibitory effect of PDG on DCM was associated with STIM1/Orai1 signaling. (A and B) The identification of si*Stim1* and si*Orai1* in H9c2 cells. (C and D) Relative mRNA expression levels of *Anp*, *Bnp*, *β-Mhc*, *Il-6*, *Tnf-α* and *Il-1β* in the Con group, HG model and *Stim1* siRNA transfected H9c2 cells following HG, HG + PDG-L, HG + PDG-M and HG + PDG-H treatment by qRT-PCR ($n$ = 4). (E and F) Relative mRNA expression levels of *Anp*, *Bnp*, *β-Mhc*, *Il-6*, *Tnf-α* and *Il-1β* in the Con group, HG model and *Orai1* siRNA transfected H9c2 cells following HG, HG + PDG-L, HG + PDG-M and HG + PDG-H treatment by qRT-PCR ($n$ = 4). (G) Flow cytometry assay images of the Con group, HG model and *Stim1* or *Orai1* siRNA transfected H9c2 cells following HG, HG + PDG-L, HG + PDG-M and HG + PDG-H treatment. (H and I) Quantification of apoptosis detected using flow cytometry ($n$ = 3). Data are shown as mean ± SD. One-way ANOVA, $^{*}P < 0.05$, $^{**}P < 0.01$ *vs* Con group; $^{\#}P < 0.05$, $^{\#\#}P < 0.01$ *vs* HG group; ns, not significant. All experiments were repeated at least three times.

STIM1/Orai1 signaling in the diabetic cellular model. Consistent with the animal experiment results, PDG had the similar inhibitory effect in the downregulation of the STIM1/Orai1 signaling *in vitro* (Figs. 7D, 7G and 7H). Meanwhile, as shown in Fig. 7I and 7L, the protein level of NFAT3 was much higher in the heart tissues in db/db mice compared to db/m mice, while PDG or Rosi

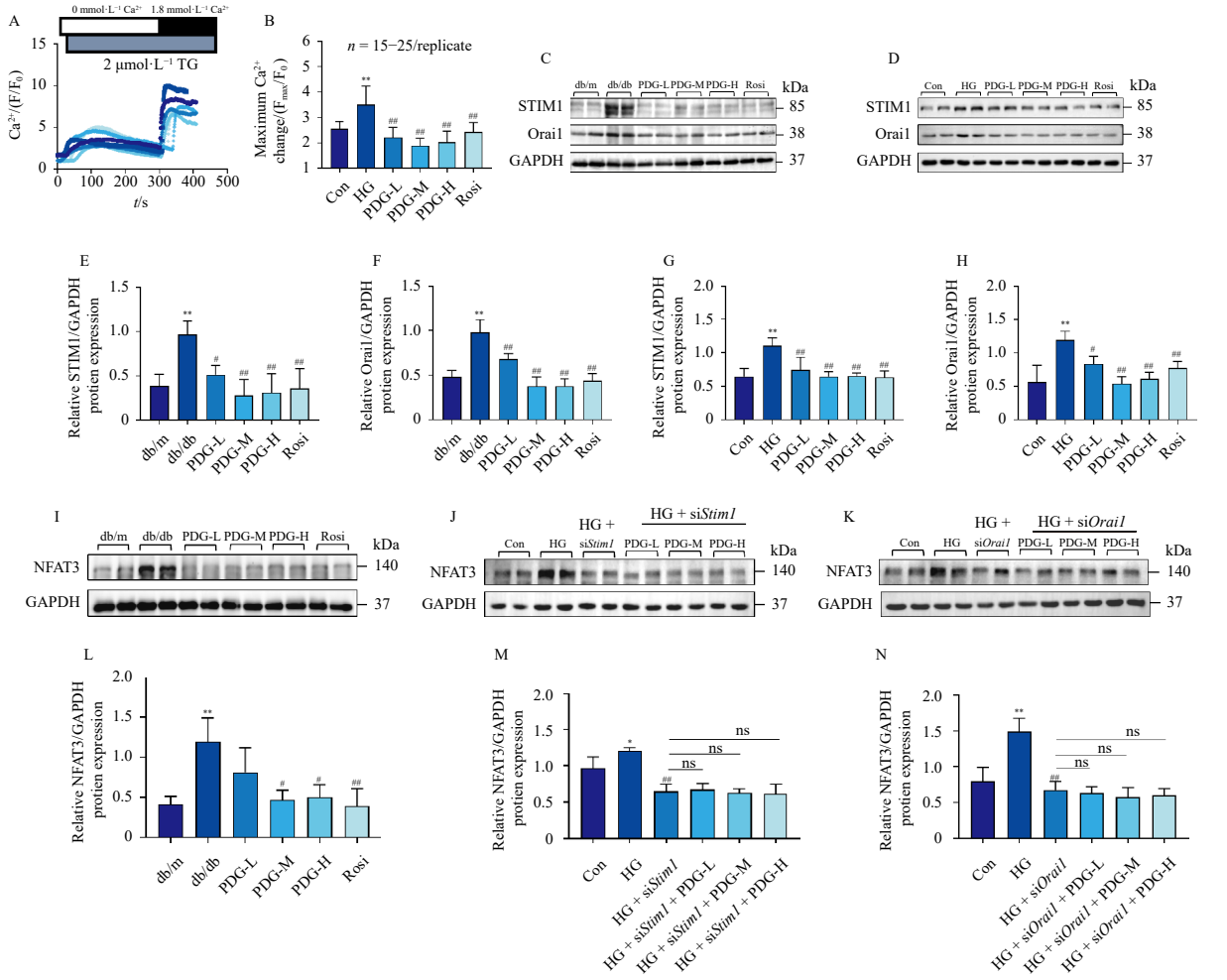



**Fig. 7** PDG suppressed SOCE and downregulated the expression of STIM1/Orai1/NFAT3 on DCM. (A and B) The effect of PDG on SOCE in HG-induced cardiomyocytes. The representative traces (left) and data summary (right) of $Ca^{2+}$ responses were shown, SOCE was plotted in the summary chart ($n$ = 15–25/replicate). (C, E and F) Western blotting and quantification of STIM1 and Orai1 in the heart tissues of mice ($n$ = 4). (D, G and H) Western blotting and quantification of STIM1 and Orai1 in H9c2 cells ($n$ = 4). (I and L) Western blotting and quantification of NFAT3 in the heart tissues of mice ($n$ = 4). (J–N) Western blotting and quantification of NFAT3 in the Con group, HG model and *Stim1* or *Orai1* siRNA transfected H9c2 cells following HG, HG + PDG-L, HG + PDG-M and HG + PDG-H treatment ($n$ = 4). Data are shown as mean ± SD. One-way ANOVA, $^{*}P < 0.05$, $^{**}P < 0.01$ *vs* db/m group or Con group; $^{\#}P < 0.05$, $^{\#\#}P < 0.01$ *vs* db/db group or HG group; ns, not significant. All experiments were repeated at least three times.

treatment obviously reversed this kind of change. Consistently, the expression of NFAT3 showed a significant increase in the HG group relative to the control group, while this kind of change could be attenuated by the deficiency of *Stim1* or *Orai1*, but PDG did not exert any additive inhibitory effect (Figs. 7J–7N). Collectively, these data indicated that PDG significantly downregulated STIM1/Orai1 signaling pathway and reduced its associated SOCE, for which negatively regulated SOCE to some extent through the activation of NFAT3 in maintaining $Ca^{2+}$ homeostasis, and ultimately inhibited the progression of DCM.

## 4. Discussion

Previous study showed that *Eucommia ulmoides* has the therapeutic effects on diabetes and some cardiovascular diseases [25]. PDG, the main constituent of *Eucommia ulmoides*, has the antihypertensive, antioxidant, and hypolipidemic effects [18]. However, the effect of PDG on DCM remains blurred. Our findings revealed that PDG effectively attenuated cardiac hypertrophy, inflammation, and cardiomyocyte apoptosis in both db/db mice and HG-induced H9c2 cells. Furthermore, we confirmed that the effect of PDG on DCM might be through suppressing the SOCE and downregulating the STIM1/Orai1 and NFAT3 signaling pathway. These data suggested that PDG has the cardioprotective role in DCM. As shown in Fig. 8, we depicted a possible schematic model with our mainly findings.

DCM is characterized by early left ventricular hypertrophy and diastolic dysfunction related to diabetes [26]. Moreover, diabetic cardiac hypertrophy could be reflected by relevant indexes, such as the cell surface area, the HW/TL ratio, and the hypertrophic responses [27]. Furthermore, diabetes-associated hyperglycemia leads to the pathological changes in the heart, such as myocardial fibrosis and hypertrophy [28]. In this study, PDG effectively improved systolic and diastolic function in db/db mice. PDG effectively suppressed cardiac hypertrophy in both animal and cell models. Overall, PDG was effective in suppressing the hypertrophic responses associated with DCM.

Inflammation is an important trigger during the development of DCM. It promotes myocardial hypertrophy and apoptosis, as well as impairs cardiac function, which assumes a key role in the pathogenesis of DCM [28]. Prolonged HG conditions lead to the secretion of inflammatory mediators from cardiomyocytes, which, in turn, promote the synthesis of pro-inflammatory cytokines, such as *Tnf-α*, *Il-1β*, and *Il-6* [29]. In this study, PDG suppressed the inflammatory responses, exhibiting a substantial reduction of the expression of *Il-6*, *Tnf-α*, and *Il-1β* at the mRNA level. These data indicated that PDG inhibited DCM-induced cardiac inflammation.

Apoptosis plays a pivotal role in the degradation of cardiac function [30]. Hyperglycemia promotes intracellular ROS production and triggers oxidative stress, which further leads to apoptosis and necrosis, eventually culminating in cardiac insufficiency,

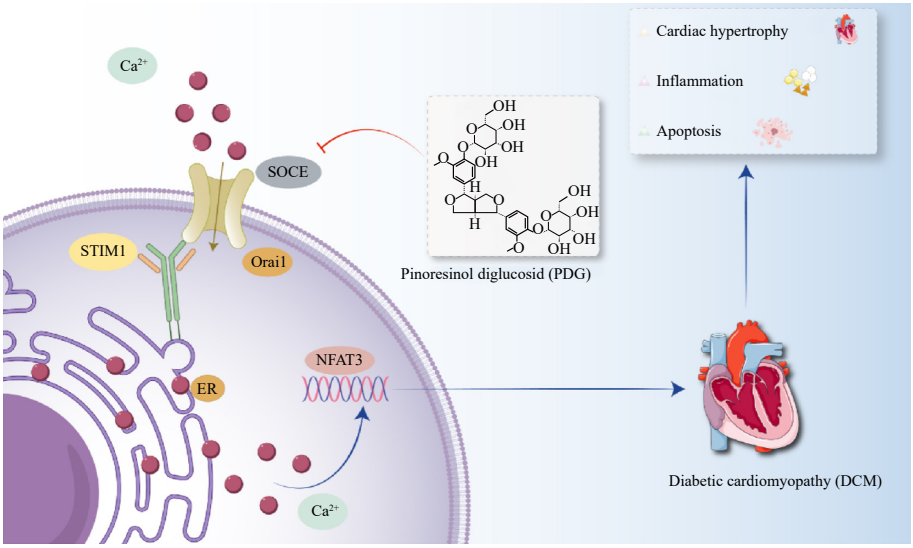



**Fig. 8** A schematic model of the possible mechanism of PDG on DCM.

remodeling, and the onset of heart failure [31]. Furthermore, hyperglycemia has the potential to induce apoptosis through the activation of caspase proteins [32]. In this context, our results indicated that PDG significantly inhibited cardiomyocyte apoptosis and the apoptotic proteins. Similarly, flow cytometry analysis further confirmed the action of PDG against apoptosis in H9c2 cells. These results indicate that PDG is effective in suppressing DCM-related apoptosis.

The mechanisms of DCM are complex, including hyperglycemia, insulin resistance, and improper intracellular calcium handling in the myocardium [33]. Recently, network pharmacology, bioinformatics, machine learning and molecular docking methods were combined to explore the possible target genes of TCM on diseases [34]. In this study, GO and KEGG enrichment analysis indicated that PDG acted on DCM by regulating the calcium signaling pathway. Machine learning algorithms identified 6 key genes including *Stim1*, *Orai1* and *Nfat3* genes, while molecular docking analysis revealed that PDG had a strong binding affinity to STIM1, Orai1 and NFAT3 proteins. Therefore, we supposed that PDG might have an interaction to STIM1/Orai1/NFAT3 signaling.

Previous studies have demonstrated that the downregulation of STIM1/Orai1 signaling and its associated SOCE can lead to inhibition of cardiac hypertrophy [35], and that inhibition of Orai1 also suppresses cardiac hypertrophy both *in vivo* and *in vitro* [36]. Moreover, disruption of cytoplasmic $Ca^{2+}$ homeostasis can exacerbate apoptosis, and inhibition of SOCE-related proteins is associated with the alleviation of HG-induced endothelial cell apoptosis [37]. Herein, our data showed that the combined deficiency of *Stim1* or *Orai1* was effective in suppressing HG-induced hypertrophy, inflammation, and apoptosis in H9c2 cells. However, these effects were not reversed after the application of PDG on this basis. The action of PDG treating DCM may be mediated through inhibition of SOCE. Therefore, our findings indicated that the inhibitory effect of PDG on DCM is associated to STIM1/Orai1 signaling and its related SOCE.

During the development of diabetic cardiac hypertrophy, the increase of $Ca^{2+}$ level triggers the activation of calcineurin/NFAT signaling pathway [38]. Pyridostigmine attenuated cardiac hypertrophy by inhibiting the expression of NFAT3 and STIM1, thereby suppressing Orai1/STIM1 complex formation [39]. In addition, HG can increase the NFATc3 level in H9c2 cells, thereby exacerbating cardiomyocyte hypertrophy and apoptosis [40]. Our results showed that PDG significantly downregulated the expression of NFAT3 at the protein level both *in vivo* and *in vitro*. Furthermore, our findings indicated that the deficiency of *Stim1* or *Orai1* downregulated the expression of NFAT3 in HG-induced H9c2 cells, but the application of PDG on the basis did not produce an additive effect. Our data revealed that inhibition of SOCE and the downregulation of STIM1/Orai1/NFAT3 signaling may be an effective target in treating T2DM-related DCM. Therefore, PDG may negatively reduce SOCE through the activation of NFAT3, in order to maintain $Ca^{2+}$ homeostasis and ultimately inhibit the progression of DCM.

Herein, our study had some limitations. This study only confirmed that the inhibitory effect of PDG on DCM caused by T2DM. Additionally, we just used network pharmacology, bioinformatics, machine learning and molecular docking methods to reveal the possible mechanism of PDG targeting DCM, and did not provide the direct interaction evidence of PDG targeting STIM1/Orai1 signaling. In the future, we would use microscale thermophoresis or surface plasmon resonance assay to identify the association between PDG and the associated proteins in the treatment of DCM.

## 5. Conclusion

PDG was effective in attenuating cardiac hypertrophy, inflammation, and apoptosis caused by DCM, potentially through the inhibition of SOCE and the downregulation of the STIM1/Orai1/NFAT3 signaling. Therefore, PDG may represent a promising therapeutic candidate for treating DCM.

## Funding

This work was supported by the Natural Science Foundation of Shandong Province (No. ZR2021LZY033), the National Natural Science Foundation of China (Nos. 81700221 and 82204391), the National Natural Science Fund for Young Scientists Fund Program (No. 82104627), the Fundamental Research Funds for the Central Universities (No. 2022-JYB-XJSJJ-065), and the National High Level Chinese Medicine Hospital Clinical Research Funding (No. DFGZRC-2024GJRC028).

## Declaration of competing interest

These authors have no conflict of interest to declare.

## References

1 Zhao X, Liu S, Wang X, et al. Diabetic cardiomyopathy: clinical phenotype and practice. *Front Endocrinol (Lausanne)*. 2022;13:1032268. https://doi.org/10.

3389/fendo.2022.1032268.
2 Huo JL, Feng Q, Pan S, et al. Diabetic cardiomyopathy: early diagnostic biomarkers, pathogenetic mechanisms, and therapeutic interventions. *Cell Death Discov*. 2023;9(1):256. https://doi.org/10.1038/s41420-023-01553-4.
3 Li W, Liu X, Liu Z, et al. The signaling pathways of selected traditional Chinese medicine prescriptions and their metabolites in the treatment of diabetic cardiomyopathy: a review. *Front Pharmacol*. 2024;15:1416403. https://doi.org/10.3389/fphar.2024.1416403.
4 Sohn P, McLaughlin MR, Krishnan P, et al. Stromal interaction molecule 1 maintains β-cell identity and function in female mice through preservation of G-protein-coupled estrogen receptor 1 signaling. *Diabetes*. 2023;72(10):1433-1445. https://doi.org/10.2337/db22-0988.
5 Rosenberg P, Zhang H, Bryson VG, et al. SOCE in the cardiomyocyte: the secret is in the chambers. *Pflugers Arch*. 2021;473(3):417-434. https://doi.org/10.1007/s00424-021-02540-3.
6 Stiber J, Hawkins A, Zhang ZS, et al. STIM1 signalling controls store-operated calcium entry required for development and contractile function in skeletal muscle. *Nat Cell Biol*. 2008;10(6):688-697. https://doi.org/10.1038/ncb1731.
7 Luo X, Hojayev B, Jiang N, et al. STIM1-dependent store-operated $Ca^{2+}$ entry is required for pathological cardiac hypertrophy. *J Mol Cell Cardiol*. 2012;52(1):136-147. https://doi.org/10.1016/j.yjmcc.2011.11.003.
8 Pang Y, Hunton DL, Bounelis P, et al. Hyperglycemia inhibits capacitative calcium entry and hypertrophy in neonatal cardiomyocytes. *Diabetes*. 2002;51(12):3461-3467. https://doi.org/10.2337/diabetes.51.12.3461.
9 Xia W, Li Y, Wang B, et al. Enhanced store-operated calcium entry in platelets is associated with peripheral artery disease in type 2 diabetes. *Cell Physiol Biochem*. 2015;37(5):1945-1955. https://doi.org/10.1159/000438555.
10 Voelkers M, Salz M, Herzog N, et al. Orai1 and Stim1 regulate normal and hypertrophic growth in cardiomyocytes. *J Mol Cell Cardiol*. 2010;48(6):1329-1334. https://doi.org/10.1016/j.yjmcc.2010.01.020.
11 Feske S. Calcium signalling in lymphocyte activation and disease. *Nat Rev Immunol*. 2007;7(9):690-702. https://doi.org/10.1038/nri2152.
12 Eguchi A, Coleman R, Gresham K, et al. GRK5 is a regulator of fibroblast activation and cardiac fibrosis. *Proc Natl Acad Sci U S A*. 2021;118(5):e2012854118. https://doi.org/10.1073/pnas.2012854118.
13 Luo Y, Jiang N, May HI, et al. Cooperative binding of ETS2 and NFAT links Erk1/2 and calcineurin signaling in the pathogenesis of cardiac hypertrophy. *Circulation*. 2021;144(1):34-51. https://doi.org/10.1161/circulationaha.120.052384.
14 He X, Wang J, Li M, et al. *Eucommia ulmoides* Oliv.: ethnopharmacology, phytochemistry and pharmacology of an important traditional Chinese medicine. *J Ethnopharmacol*. 2014;151(1):78-92. https://doi.org/10.1016/j.jep.2013.11.023.
15 Li L, Su C, Chen X, et al. Chlorogenic acids in cardiovascular disease: a review of dietary consumption, pharmacology, and pharmacokinetics. *J Agric Food Chem*. 2020;68(24):6464-6484. https://doi.org/10.1021/acs.jafc.0c01554.
16 Zhang Y, Lei Y, Yao X, et al. Pinoresinol diglucoside alleviates ischemia/reperfusion-induced brain injury by modulating neuroinflammation and oxidative stress. *Chem Biol Drug Des*. 2021;98(6):986-996. https://doi.org/10.1111/cbdd.13956.
17 Luo LF, Wu WH, Zhou YJ, et al. Antihypertensive effect of *Eucommia ulmoides* Oliv. extracts in spontaneously hypertensive rats. *J Ethnopharmacol*. 2010;129(2):238-243. https://doi.org/10.1016/j.jep.2010.03.019.
18 Yuan W, Liang X, Liu YY, et al. Pinoresinol diglucoside ameliorates H/R-induced injury of cardiomyocytes by regulating miR-142-3p and HIF1AN. *J Biochem Mol Toxicol*. 2022;36(10):e23175. https://doi.org/10.1002/jbt.23175.
19 Chen Y, Pan R, Zhang J, et al. Pinoresinol diglucoside (PDG) attenuates cardiac hypertrophy *via* AKT/mTOR/NF-κB signaling in pressure overload-induced rats. *J Ethnopharmacol*. 2021;272:113920. https://doi.org/10.1016/j.jep.2021.113920.
20 Li H, Wang X, Mao Y, et al. Long term liver specific glucokinase gene defect induced diabetic cardiomyopathy by up regulating NADPH oxidase and down regulating insulin receptor and p-AMPK. *Cardiovasc Diabetol*. 2014;13:24. https://doi.org/10.1186/1475-2840-13-24.
21 Yang F, Luo G, Liu MN, et al. Network pharmacology and experimental validation to investigate the mechanism of action of Zhilong Huoxue Tongyu Capsule in the prevention and treatment of diabetic cardiomyopathy. *PLoS One*. 2025;20(5):e0323745. https://doi.org/10.1371/journal.pone.0323745.
22 Liu M, Wang Y, Deng W, et al. Combining network pharmacology, machine learning, molecular docking and molecular dynamic to explore the mechanism of Chufeng Qingpi Decoction in treating schistosomiasis. *Front Cell Infect Microbiol*. 2024;14:1453529. https://doi.org/10.3389/fcimb.2024.1453529.
23 Li C, Wen R, Liu D, et al. Assessment of the potential of *Sarcandra glabra* (Thunb) Nakai. in treating ethanol-induced gastric ulcer in rats based on metabolomics and network analysis. *Front Pharmacol*. 2022;13:810344. https://doi.org/10.3389/fphar.2022.810344.
24 Suriano F, Vieira-Silva S, Falony G, et al. Novel insights into the genetically obese (ob/ob) and diabetic (db/db) mice: two sides of the same coin. *Microbiome*. 2021;9(1):147. https://doi.org/10.1186/s40168-021-01097-8.
25 Huang L, Lyu Q, Zheng W, et al. Traditional application and modern pharmacological research of *Eucommia ulmoides* Oliv.. *Chin Med*. 2021;16(1):73. https://doi.org/10.1186/s13020-021-00482-7.
26 Paolillo S, Marsico F, Prastaro M, et al. Diabetic cardiomyopathy: definition, diagnosis, and therapeutic implications. *Heart Fail Clin*. 2019;15(3):341-347. https://doi.org/10.1016/j.hfc.2019.02.003.
27 Fang T, Wang J, Sun S, et al. JinLiDa Granules alleviates cardiac hypertrophy and inflammation in diabetic cardiomyopathy by regulating TP53. *Phytomedicine*. 2024;130:155659. https://doi.org/10.1016/j.phymed.2024.155659.
28 Jia G, Hill MA, Sowers JR. Diabetic cardiomyopathy: an update of mechanisms contributing to this clinical entity. *Circ Res*. 2018;122(4):624-638. https://doi.org/10.1161/circresaha.117.311586.
29 Mori J, Patel VB, Abo AO, et al. Angiotensin 1-7 ameliorates diabetic cardiomyopathy and diastolic dysfunction in db/db mice by reducing lipotoxicity and inflammation. *Circ Heart Fail*. 2014;7(2):327-339. https://doi.org/10.1161/circheartfailure.113.000672.
30 Su D, Gao Q, Guan L, et al. Downregulation of SOX11 in fetal heart tissue, under hyperglycemic environment, mediates cardiomyocytes apoptosis. *J Biochem Mol Toxicol*. 2021;35(1):e22629. https://doi.org/10.1002/jbt.22629.
31 Jubaidi FF, Zainalabidin S, Taib IS, et al. The potential role of flavonoids in ameliorating diabetic cardiomyopathy *via* alleviation of cardiac oxidative stress, inflammation and apoptosis. *Int J Mol Sci*. 2021;22(10):5094. https://doi.org/10.3390/ijms22105094.
32 Sun S, Yang S, Dai M, et al. The effect of Astragalus polysaccharides on attenuation of diabetic cardiomyopathy through inhibiting the extrinsic and intrinsic apoptotic pathways in high glucose -stimulated H9C2 cells. *BMC Complement Altern Med*. 2017;17(1):310. https://doi.org/10.1186/s12906-017-1828-7.
33 Li J, Richmond B, Cluntun AA, et al. Cardiac gene therapy treats diabetic cardiomyopathy and lowers blood glucose. *JCI Insight*. 2023;8(18):e166713. https://doi.org/10.1172/jci.insight.166713.
34 Huang W, He C, Kim HI, et al. MMP3 as a new target of Danshensu/tetramethylpyrazine derivative for attenuating cardiac fibrosis post-myocardial infarction. *Life Sci*. 2025;370:123570. https://doi.org/10.1016/j.lfs.2025.123570.
35 Liu X, Chang Y, Choi S, et al. Blocking store-operated $Ca^{(2+)}$ entry to protect HL-1 cardiomyocytes from epirubicin-induced cardiotoxicity. *Cells*. 2023;12(5):723. https://doi.org/10.3390/cells12050723.
36 Wu QR, Zheng DL, Liu PM, et al. High glucose induces Drp1-mediated mitochondrial fission *via* the Orai1 calcium channel to participate in diabetic cardiomyocyte hypertrophy. *Cell Death Dis*. 2021;12(2):216. https://doi.org/10.1038/s41419-021-03502-4.
37 Lu T, Zhou D, Gao P, et al. Resveratrol attenuates high glucose-induced endothelial cell apoptosis *via* mediation of store-operated calcium entry. *Mol Cell Biochem*. 2018;442(1-2):73-80. https://doi.org/10.1007/s11010-017-3194-7.
38 Kuo WW, Chung LC, Liu CT, et al. Effects of insulin replacement on cardiac apoptotic and survival pathways in streptozotocin-induced diabetic rats. *Cell Biochem Funct*. 2009;27(7):479-487. https://doi.org/10.1002/cbf.1601.
39 Lu Y, Zhao M, Liu JJ, et al. Long-term administration of pyridostigmine attenuates pressure overload-induced cardiac hypertrophy by inhibiting calcineurin signalling. *J Cell Mol Med*. 2017;21(9):2106-2116. https://doi.org/10.1111/jcmm.13133.
40 Marthandam AS, Yang JY, Lin WT. Anti-hypertrophic and anti-apoptotic effects of short peptides of potato protein hydrolysate against hyperglycemic condition in cardiomyoblast cells. *Biomed Pharmacother*. 2018;107:1667-1673. https://doi.org/10.1016/j.biopha.2018.08.070.